Inorg. Chem. **2008**, *47*, 9372−9379

Density Functional Theory Study of the Structural, Electronic, and Magnetic Properties of a μ-oxo Bridged Dinuclear Fe^{IV} Complex Based on a Tetra-Amido Macrocyclic Ligand

Arani Chanda, Filipe Tiago de Oliveira, Terrence J. Collins,* Eckard Münck,* and Emile L. Bominaar*

Department of Chemistry, Carnegie Mellon University, Pittsburgh, Pennsylvania, 15213

Received May 14, 2008

Recently, the synthesis, crystallographic structure, and Mössbauer characterization of the first example of an $[(Fe^{IV}TAML)_2O]^{2-}$ (TAML = tetra-amido microcyclic ligand) complex were reported. Here, we elucidate the prominent structural, electronic, and magnetic properties of this complex on the basis of density functional theory (DFT) calculations. While the torsion between the molecular halves is caused by hydrogen bonding between the TAML moieties, the bending of the Fe−O−Fe unit is an intrinsic property of the bridge. The values for the ^{57}Fe isomer shift and quadrupole splitting obtained with DFT are in good agreement with experimental results and indicate that the irons have intermediate spin states ($S_1 = S_2 = 1$). The iron spins are coupled by strong antiferromagnetic exchange to yield a ground state with system spin $S = 0$. The Fe−O distances in the excited $S > 0$ states are significantly longer than in the ground state. Since the wave function of the ground state, in which the iron spins are antiferromagnetically coupled to give system spin $S = 0$, is a linear combination of Slater determinants that cannot be treated with existing DFT codes, the Fe−O distance for the $S = 0$ state has been estimated by extrapolation from the optimized geometries for the ferromagnetic state ($S = 2$) and the broken symmetry state to be 1.748 Å, in good agreement with the crystallographic distance 1.728 Å. To accommodate the spin-dependent reorganization energies, the conventional bilinear spin Hamiltonian has been extended with a biquadratic coupling term: $\hat{H}_{ex} = c' + j_0\hat{\mathbf{S}}_1 \cdot \hat{\mathbf{S}}_2 + j_1(\hat{\mathbf{S}}_1 \cdot \hat{\mathbf{S}}_2)^2$. A computational scheme is presented for estimating the exchange parameters, yielding the values $j_0 = 199$ cm^{-1} and $j_1 = -61$ cm^{-1} for $[(Fe^{IV}B^*)_2O]^{2-}$. Two mechanisms for biquadratic exchange are discussed.

1. Introduction

The combination of an electron-rich tetra-amido microcyclic ligand (TAML) coordination environment and a noncoordinating aprotic medium allows Fe^{III} to activate molecular oxygen to produce high-valent $[(Fe^{IV}TAML)_2O]^{2-}$ complexes.[1] Two of these systems have been structurally and spectroscopically characterized and are, together with a complex reported by Wieghardt and co-workers,[2] the only singly bridged bis(Fe^{IV})-μ-oxo species known to date. While computational studies for the large class of bis(Fe^{III})-μ-oxo[3−9] compounds and the bis(Fe^{IV})-bis(μ-oxo) intermediate in methane monooxygenase[10−12] are available in the literature, an analysis of bis(Fe^{IV})-μ-oxo species with a single,

* Authors to whom correspondence should be addressed. E-mail: tc1u@andrew.cmu.edu (T.J.C.), emunck@cmu.edu (E.M.), eb7g@andrew.cmu.edu (E.L.B.).

(1) Ghosh, A.; Tiago de Oliveira, F.; Yano, T.; Nishioka, T.; Beach, E. S.; Kinoshita, I.; Münck, E.; Ryabov, A. D.; Horwitz, C. P.; Collins, T. J. *J. Am. Chem. Soc.* **2005**, *127*, 2505–2513.
(2) Vogel, E.; Will, S.; Tilling, A. S.; Neumann, L.; Lex, J.; Bill, E.; Trautwein, A. X.; Wieghardt, K. *Angew. Chem., Intl. Ed.* **1994**, *33*, 731–735.
(3) Gorun, S. M.; Lippard, S. J. *Inorg. Chem.* **1991**, *30*, 1625–1630.
(4) Kurtz, D. M., Jr. *Chem. Rev.* **1990**, *90*, 585–606.
(5) Lee, D.; Pierce, B.; Krebs, C.; Hendrich, M. P.; Huynh, B. H.; Lippard, S. J. *J. Am. Chem. Soc.* **2002**, *124*, 3993–4007.
(6) Lee, D.; Du Bois, J.; Petasis, D.; Hendrich, M. P.; Krebs, C.; Huynh, B. H.; Lippard, S. J. *J. Am. Chem. Soc.* **1999**, *121*, 9893–9894.
(7) Jullien, J.; Juhasz, G.; Mialane, P.; Dumas, E.; Mayer, C. R.; Marrot, J.; Rivière, E.; Bominaar, E. L.; Münck, E.; Sécheresse, F. *Inorg. Chem.* **2006**, *45*, 6922–6927.
(8) Hart, J. R.; Rappe, A. K.; Gorun, S. M.; Upton, T. H. *Inorg. Chem.* **1992**, *31*, 5253–5259.
(9) Chen, Z.; Xu, Z.; Zhang, L.; Yan, F.; Lin, Z. *J. Phys. Chem. A* **2001**, *105*, 9710–9716.
(10) Musaev, D. G.; Basch, H.; Morokuma, K. *J. Am. Chem. Soc.* **2002**, *124*, 4135–4148.
(11) Siegbahn, P. E. M.; Crabtree, R. H. *J. Am. Chem. Soc.* **1997**, *119*, 3103–3113.
(12) Baik, M.-H.; Gherman, B. F.; Friesner, R. A.; Lippard, S. J. *J. Am. Chem. Soc.* **2002**, *124*, 14608–14615.

10.1021/ic800881p CCC: $40.75
Published on Web 09/26/2008

unsupported oxo bridge is hitherto lacking. To fill this void, we present here an extensive density functional theory (DFT) investigation of the structural, electronic, and magnetic properties of the complex $[(Fe^{IV}B^*)_2O]^{2-}$. The present work is a continuation of our computational studies of mononuclear Fe^{IV}−TAML complexes, which have been reviewed recently.[13]

2. Methods and Materials

2.1. List of Acronyms for Ligands. H_4B^*: 7,7,10,10,13,13-hexamethyl-5,7,8,12,13,15-hexahydro-5,8,12,15-tetraazabenzocyclotridecen-6,9,11,14-tetraone. H_4DMOB: 10,10-diethyl-2,3-dimethoxy-7,7,13,13-tetramethyl-5,7,8,12,13,15-hexahydro-5,8,12,15-tetraazabenzocyclotridecene-6,9,11,14-tetraone. H_4MAC^*: 6,6-diethyl-3,3,9,9,12,12,14,14-octamethyl-1,4,8,11-tetraazacyclotetradecane-2,5,7,10,13-pentaone. TMC: 1,4,8,11-tetramethyl-1,4,8,11-tetraazacyclotetradecane.

2.2. Computational Details. The DFT calculations were performed with the Gaussian 03 code, revision B.05,[14] using the hybrid functional B3LYP.[15,16] The calculation for obtaining the molecular geometry shown in Figure 1D is discussed below and in section 3.3.1. The results presented in Table 1 and Figure 2 were obtained with the triple-ζ basis set 6-311G. Table 1 lists key structural data obtained from geometry optimizations for the $S = 2$ states of the models shown in Figure 2. The models are shown in their optimized conformations. Although the optimizations of Figure 2 did not impose any geometrical symmetry constraints, they resulted in C_2 symmetric conformations. Default convergence criteria were used, unless mentioned otherwise.

The calculations for $[(B^*Fe^{IV})_2O]^{2-}$, described in section 3.3.1, were performed with the basis set 6-311G*, which is obtained from basis 6-311G by the addition of polarization functions for the heavy atoms. Since the equilibrium conformations obtained for basis 6-311G have C_2 symmetry, we imposed this symmetry in the 6-311G* geometry optimizations to expedite the calculations. The geometry optimization for the $S = 2$ state was terminated upon reaching the default convergence criteria for the forces and the root-mean-square (rms) displacement. The maximum displacement criterion was relaxed to 0.00062 Å (default 0.00018 Å), corresponding to a minor error of ∼1 cm^{-1} in the total energy. Vibrational analysis, using the FREQ keyword, for the optimized structure yielded exclusively real frequencies, indicating that the stationary point found in the optimization is a minimum. Subsequently, a broken symmetry (BS) state for the $S = 2$ geometry was constructed as previously described.[17,18] This state was used as the initial guess for a single-point calculation, which was readily converged using tight self-consistent field (SCF) criteria. Time-dependent DFT calculation (TD keyword) for the BS state resulted in exclusively positive excitation energies, corroborating that we secured the DFT solution with the lowest energy obtainable for a spin-unrestricted configuration with equal numbers of spin-up and -down electrons. The BS approach adopted here was previously applied to a number of diiron(III) complexes with unsupported μ-oxo and μ-hydroxo bridges and provided a good description of the exchange-coupling constants in these systems.[7] The SCF energies for the $S = 2$ and BS states were scanned along the Fe−O coordinate. The resulting potential energy surfaces (PES) are shown in Figures S1−S2 (Supporting Information), together with parabolic fits, which have been collected in Figure 4 for comparison. The BS character of the lowest DFT state has been verified with a Mulliken population analysis of the atomic spin populations (SPs). The SPs of the two iron atoms are ±1.95 in the BS state and +2.19 in the $S = 2$ state and are close to the value $|SP| = 2$ expected for the spin triplet states of the irons. The corresponding spin densities for B* are ±0.15 in the BS state and −0.28 for $S = 2$. Addition of the spin populations of iron, B*, and half the $SP = 0.18$ for the bridging oxo ligand yields for the $S = 2$ state a total spin density of 2 for each molecular half; the analogous addition for the BS state gives a smaller total value ($SP = 1.80$) since the spin densities at the oxo bridge cancel: $SP = 0$ for μ-oxo in the BS state. The SP values show only a moderate dependence on Fe−O distance in the range considered here. The numbers listed here were obtained at an Fe−O distance of 1.76 Å for the two spin states with basis 6-311G*. The spin densities are discussed in more detail in section 3.3.2.

The observables listed in Table 2 have been calculated for the BS state at an Fe−O distance 1.748 Å, that is, the minimum of the PES for the $S = 0$ state described in section 3.3.1. The electric field gradients at the Fe nuclei were calculated, using the PROPERTIES keyword of Gaussian, and converted to millimeters per second, by multiplication with the conversion factor −1.6 (mm/s)/AU, which corresponds to a value of 0.16 b for the nuclear quadrupole moment of the $I = 3/2$ excited state of the ^{57}Fe nucleus. To calculate the isomer shift, we projected the BS solution for 6-311G* onto the 6-311G basis and reconverged the SCF procedure to obtain the BS state for the smaller basis set. This solution was used to calculate the electron densities at Fe nuclei from which the isomer shift δ was evaluated using the 6-311G-based calibration of Vrajmasu et al.[19]

3. Results and Discussion

3.1. Structural Properties. Two $[(Fe^{IV}TAML)_2O]^{2-}$ complexes have been reported to date, namely, the species with the TAML ligands B* and DMOB* (i.e., the dimethoxy adduct of B*; see the caption of Figure 1A). These complexes have the following structural features in common: (i) the TAML moieties are rotated relative to each other over a torsion angle $\varphi = \angle C_1Fe_1Fe_2C_2$ of about 50° when viewed along the Fe···Fe vector, where C_1 and C_2 are the tail

(13) Chanda, A.; Popescu, D.-L.; Tiago de Oliveira, F.; Bominaar, E. L.; Ryabov, A. D.; Münck, E.; Collins, T. J. *J. Inorg. Biochem.* **2006**, *100*, 606–619.

(14) Frisch, M. J.; Trucks, G. W.; Schlegel, H. B.; Scuseria, G. E.; Robb, M. A.; Cheeseman, J. R.; Montgomery, J. A. J.; Vreven, T.; Kudin, K. N.; Burant, J. C.; Millam, J. M.; Iyengar, S. S.; Tomasi, J.; Barone, V.; Mennucci, B.; Cossi, M.; Scalmani, G.; Rega, N.; Petersson, G. A.; Nakatsuji, H.; Hada, M.; Ehara, M.; Toyota, K.; Fukuda, R.; Hasegawa, J.; Ishida, M.; Nakajima, T.; Honda, Y.; Kitao, O.; Nakai, H.; Klene, M.; Li, X.; Knox, J. E.; Hratchian, H. P.; Cross, J. B.; Bakken, V.; Adamo, C.; Jaramillo, J.; Gomperts, R.; Stratmann, R. E.; Yazyev, O.; Austin, A. J.; Cammi, R.; Pomelli, C.; Ochterski, J. W.; Ayala, P. Y.; Morokuma, K.; Voth, G. A.; Salvador, P.; Dannenberg, J. J.; Zakrzewski, V. G.; Dapprich, S.; Daniels, A. D.; Strain, M. C.; Farkas, O.; Malick, D. K.; Rabuck, A. D.; Raghavachari, K.; Foresman, J. B.; Ortiz, J. V.; Cui, Q.; Baboul, A. G.; Clifford, S.; Cioslowski, J.; Stefanov, B. B.; Liu, G.; Liashenko, A.; Piskorz, P.; Komaromi, I.; Martin, R. L.; Fox, D. J.; Keith, T.; Al-Laham, M. A.; Peng, C. Y.; Nanayakkara, A.; Challacombe, M.; Gill, P. M. W.; Johnson, B.; Chen, W.; Wong, M. W.; Gonzalez, C.; Pople, J. A. *Gaussian 03*, revision B.05; Gaussian, Inc.: Wallingford, CT, 2004.

(15) Becke, A. D. *J. Chem. Phys.* **1993**, *98*, 5648–5652.

(16) Lee, C.; Yang, W.; Parr, R. G. *Phys. Rev. B: Condens. Matter Mater. Phys.* **1988**, *37*, 785–789.

(17) Eckert, N. A.; Stoian, S.; Smith, J. M.; Bominaar, E. L.; Münck, E.; Holland, P. L. *J. Am. Chem. Soc.* **2005**, *127*, 9344–9345.

(18) Noodleman, L. *J. Chem. Phys.* **1981**, *74*, 5737–5743.

(19) Vrajmasu, V.; Münck, E.; Bominaar, E. L. *Inorg. Chem.* **2003**, *42*, 5974–5988.

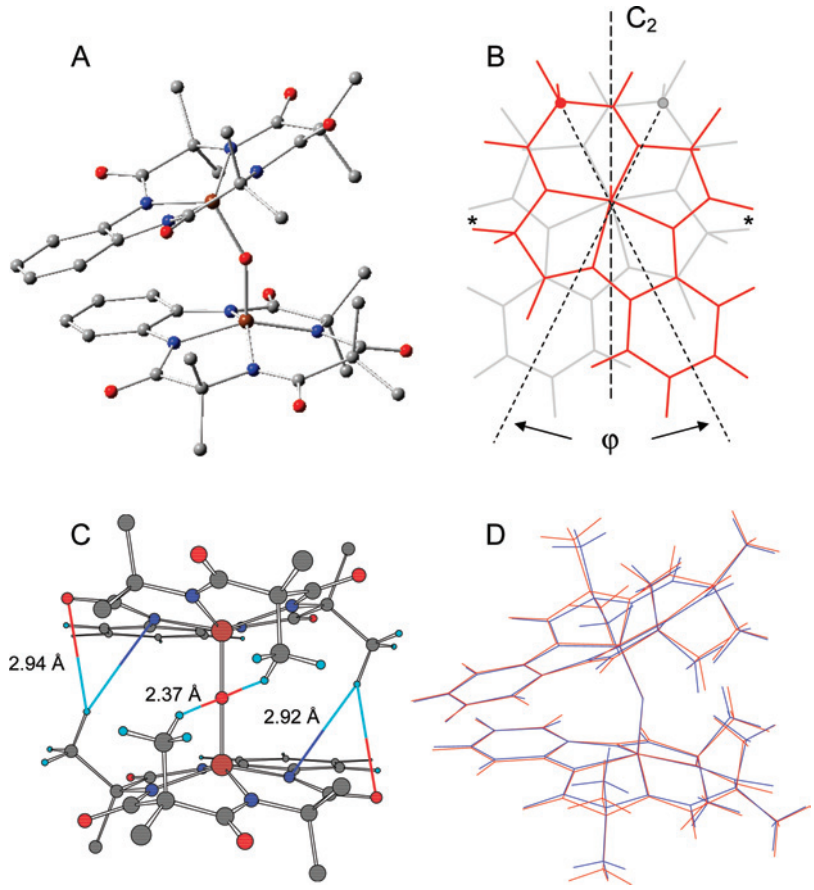

Figure 1. (A) Crystallographic structure of $[(Fe^{IV}B^*)_2O]^{2-}$. Hydrogens have been omitted for clarity. DMOB* is obtained from B* by adding methoxy groups at positions 3 and 4 of the benzene ring. Color code: blue (N), brown (Fe), gray (C), and red (O). Parameters: Fe−O = 1.728 Å (1.737 Å), $\varphi = 54.0°$ (46.0°), Fe−O−Fe = 151.4° (153.8°) for B* (DMOB*). (B) View of molecule along the Fe···Fe vector, showing torsion angle $\varphi = C_1{-}Fe_1{-}Fe_2{-}C_2$. The tail carbons C_1 and C_2 are indicated by dots. The C_2 axis runs through the μ-oxo center. The * indicates the locations of the outermost hydrogen bonds of 1C. (C) View along the pseudo C_2 axis of the molecule. All hydrogens of methyls engaged in interligand hydrogen bonding are displayed. Only hydrogen bonds between the ligands with distances < 3 Å have been indicated. (D) Overlay of the X-ray structure (blue) and the geometry predicted for the $S = 0$ ground state (red) on the basis of DFT calculations; for details, see section 3.3.1. The overlay minimizes the rmsd between the $N_4FeOFeN_4$ units in the two structures.

carbons of the TAML ligands (Figure 1B), and (ii) the Fe−O−Fe bridge is bent with an angle of about 150° (Figure 1A). The torsion angle φ lowers the molecular symmetry from C_{2v} ($\varphi = 0°$) to C_2 ($\varphi > 0°$). The C_2 axis bisects the Fe−O−Fe angle (Figure 1B); a view of the complex along the symmetry axis is given in Figure 1C. Given the similarity between the two complexes, we have focused our computational efforts on one of them, namely, the B* complex.

3.1.1. Origin of Torsion φ Figure 2 defines a number of structures, including the original complex (model 4) and truncated complexes (models 1−3, 5−8). Models 1−3 are obtained by substituting the tail or side methyls of model 4 with hydrogens; models 5−8 follow from models 1−4 by replacing the benzenes with alkenes. The geometries of these models have been optimized using DFT (see section 2). The resulting torsion angles, listed in Table 1, show the following trends: (1) The methyl-free models 1 and 5 have large torsion angles, indicating that the steric repulsions associated with the close contacts between the methyls for $\varphi = 0°$ are not the only origin for the torques acting on the TAML moieties in C_{2v} symmetry. (2) The presence of the benzene in model 1 increases the torsion angle relative to the one for model 5 by 37°. (3) Addition of the tail methyls to models 1 and 5 has little effect on the torsion angle in model 2 and gives only a slight increase in model 6, due to the large torsions already present in the absence of the methyls. (4) The values for φ in models 1, 2, 5, and 6 are rather dispersed and agree poorly with the experimental value, $\varphi = 54°$. (5) The torsion angles $\varphi \approx 54°$ for the optimized structures of the side methyls containing models 3, 4, 7, and 8 are in excellent agreement with experiment. The insensitivity of the torsion angle on the modifications that differentiate the latter models indicates that the side methyls are engaged in the dominant interactions between the ligands of model 4. As illustrated in Figure 1B and C, a torsion angle of 54° juxtaposes one of the interior side methyls of a ligand to one of the carbonyl groups closest to the head (benzene) of the opposite ligand in a way favorable for hydrogen bonding. The H···O=C distance of 2.920 Å, while on the long side, is well within the established hydrogen-bonding range.[20] The two H···O=C distances between the side methyls and the carbonyls closest

(20) Hamilton, W. C.; Ibers, J. A. *Hydrogen Bonding in Solids, Methods of Molecular Structure Determination (Frontiers in Chemistry)*; 1968; p 284.

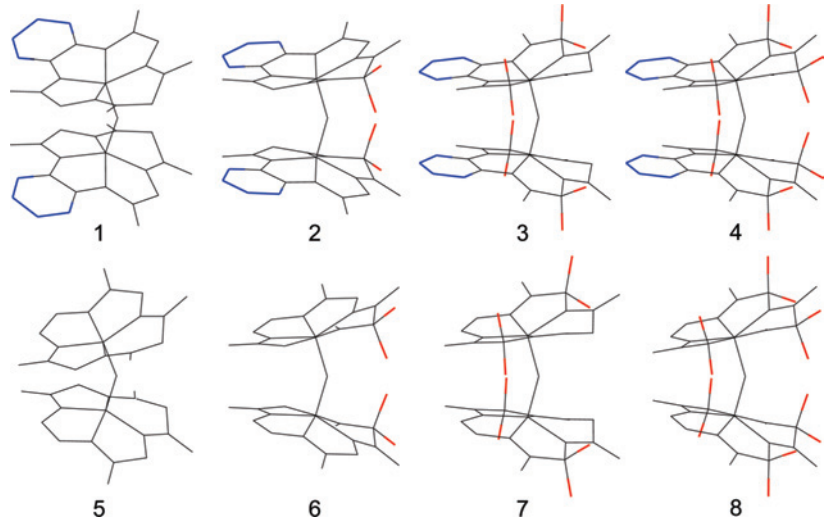

Figure 2. Model **4** represents the structure of $[(Fe^{IV}B^*)_2O]^{2-}$; models **1**−**3** and **5**−**8** are structural modifications. Red, methyl groups; blue, section of benzene removed in the bottom half of the figure. Hydrogens have been omitted for clarity. Each model is shown in the optimized conformation and viewed from the same perspective relative to the Fe−O−Fe unit. The enantiomer shown in this figure is complementary to the one of Figure 1. Values for the structural parameters for the Fe−O−Fe unit and the torsion angle φ are listed in Table 1.

Table 1. Bond Length, Bond Angle, and Torsion Angle from DFT[a] for Models of Figure 2

complex	model complex		Fe−O (Å)	Fe−O−Fe (deg)	torsion angle, φ (deg)
1	benzene	no methyls	1.778	147.8	103.9
2		tail methyls	1.783	145.0	102.6
3		side methyls [b]	1.795	152.3	49.2
4		side and tail methyls	1.818	154.5	53.5
5	alkene	no methyls	1.797	148.2	67.3
6		tail methyl	1.807	148.7	74.5
7		side methyl	1.805	151.2	56.4
8		side and tail methyls	1.825	150.3	60.8
	X-ray	side and tail methyls	1.728	151.4	54.0

[a] Obtained with B3LYP/6-311G for $S = 2$. [b] Optimization with B3LYP/6-31G for $S = 2$.

to the tail are considerably larger than 3 Å.[21] We conclude from these results that hydrogen bonding is the driving force responsible for the torsion angle between the TAML moieties.

3.1.2. Origin of Fe−O−Fe Bending. The geometry optimization of $[(Fe^{IV}B^*)_2O]^{2-}$ yields for the Fe−O−Fe angle the value 153°, which is in good agreement with the angle 151° obtained from the crystallographic analysis of this complex.[1] The crystal structure as well as the optimized structure reveal the presence of hydrogen bonding between the tail methyls and the oxo bridge (2.37 Å, Figure 1C), suggesting a potential role of this interaction in the bending of the bridge. However, this possibility can be ruled out since replacement of the tail methyls with hydrogens (models **3** and **7**) has virtually no effect on the Fe−O−Fe angle. Similarly, the other ligand modifications considered in Figure 2, which alter the interactions between the ligands (see section 3.1.1), have no significant influence on the Fe−O−Fe angle either. These results suggest that the bent Fe−O−Fe conformation is an intrinsic property of this unit, which can be explained as follows.

Coordinative bonds involve the donation of electron density from the ligands into the vacant 3d orbitals of the metal ion. The empty z^2 orbitals (see section 3.2), which are directed toward the bridging oxygen (Figure 3), are the primary receptors of electron density donated by the oxo ligand. Figure 3 considers two conformations: the linear conformation (A) and the orthogonal conformation (B). The conformation affects the way in which the two Fe−O coordination bonds of the dimer interfere with one another. In the linear conformation, the irons receive electron density

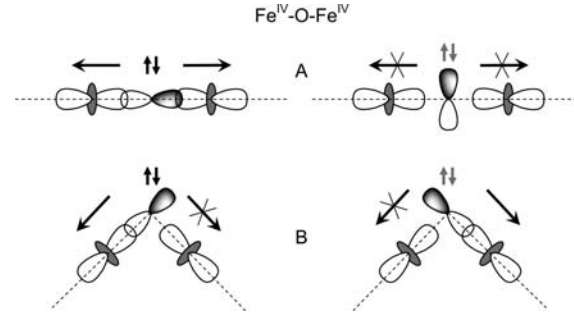

Figure 3. Diagrams displaying two atomic z^2-type orbitals at the irons and one atomic p orbital at the bridging oxygen in (A) linear and (B) orthogonal conformations. The z^2 orbitals are directed toward the bridging oxygen; the p orbitals are chosen such that they either maximize or minimize the overlap with a z^2 orbital. Before the transfer interactions are turned on, the z^2-type orbitals are empty and the p orbitals are doubly occupied. The long arrows indicate allowed and forbidden (crossed arrows) oxygen-to-metal electron donations. The electrons of oxygen occupying different p orbitals are shown in different shadings. In the linear conformation (A), the two z^2-type orbitals compete for electron density from the *same* p orbital, whereas in the orthogonal conformation (B), they draw electron density from *different* p orbitals, leading to stronger bonding energies in B.

(21) These distances are ∼3.9 Å in the B* complex; in the DMOB* complex, they have different values, 3.9 and 3.1 Å, due to a distortion of the C_2 symmetry.

Table 2. Experimental and DFT Calculated Mössbauer Parameters and Spin States

Complex	local spin		ΔE_Q (mm/s)	δ (mm/s)
$[(Fe^{IV}B^*)_2O]^{2-}$	$S_1 = S_2 = 1$	exp.	+3.3	−0.07
		DFT	+3.5	−0.03
$[Fe^{IV}MAC^*(Cl)]^-$	$S = 2$	exp.	−0.89	−0.04

from the same electron pair (Figure 3A), whereas in the orthogonal conformation, the irons communicate with different electron pairs (Figure 3B). As a consequence, the orthogonal conformation gives stronger Fe−O bonds and a lower energy. The energy minimum for the orthogonal conformation is supported by a simple Hückel analysis, for which the details are presented in the Supporting Information. The model in Figure 3 ignores π bonding and any s−p hybridization at the oxygen, which, if present, would yield a larger bond angle, like in the water molecule.

3.2. Electronic Properties. The ^{57}Fe isomer shifts (δ) and the quadrupole splittings (ΔE_Q) for $[(Fe^{IV}B^*)_2O]^{2-}$ obtained from Mössbauer spectroscopy[1] and our DFT calculations have been listed in Table 2. A comparison shows that the calculated values are in good agreement with experimental results. Table 2 also presents the electric hyperfine parameters for the mononuclear complex $[Fe^{IV}MAC^*(Cl)]^-$.[22] The remarkable difference in the quadrupole splittings for the two species can be explained as follows. The MAC* complex has a high-spin ($S = 2$) ground state with the idealized 3d configuration $(xy)^1(xz)^1(yz)^1(z^2)^1$, where the z axis is defined along the Fe−Cl axis and the x and y axes are directed toward the amido nitrogens.[13] This configuration is obtained by removing the x^2-y^2 electron from a half-filled 3d shell and gives therefore a large, negative valence contribution (ca. −4 mm/s) to ΔE_Q. Mulliken population analyses of the DFT solutions show that the amido groups donate substantial electron density into the x^2-y^2 orbital, contributing a large, positive ligand term (ca. +3 mm/s) to ΔE_Q. The valence and ligand contributions to ΔE_Q give together a total of ca. −1 mm/s for the quadrupole splitting of the $S = 2$ species (see Table 2). Let us now consider binuclear species $[(Fe^{IV}B^*)_2O]^{2-}$. Since μ-oxo is a stronger ligand than chloride, the z^2 level in $[(Fe^{IV}B^*)_2O]^{2-}$ is raised in energy relative to the z^2 level in $[Fe^{IV}MAC^*(Cl)]^-$, forcing the electron in this orbital to pair off with the electron in the low-lying xy orbital, leading to 3d configuration $(xy)^2(xz)^1(yz)^1$ for the Fe^{IV} sites of the dimer. These intermediate-spin Fe^{IV} states have been identified in the DFT solutions for both the broken-symmetry and ferromagnetic states of the dimer, based on Mulliken gross orbital population analysis. The $(xy)^2(xz)^1(yz)^1$ configuration yields a valence contribution of ca. +4 mm/s to ΔE_Q. Given that the Fe^{IV}−N(amide) bonds in the two complexes have virtually equal lengths, the ligand contributions associated with the charge donations into x^2-y^2 are expected to be equal as well (+3 mm/s), leading to a total of $\Delta E_Q \approx +7$ mm/s. However, since μ-oxo is a much stronger electron donor than chloride, the former ligand gives a much larger axial contribution to ΔE_Q than the latter. The axial ligand contribution is negative, since z^2 is the principal acceptor orbital and has a value of about −4 mm/s in the μ-oxo complex. Summing the three contributions yields the total $\Delta E_Q \approx +3$ mm/s for $[(Fe^{IV}B^*)_2O]^{2-}$ (see Table 2). Thus, the quadrupole splitting gives a unique signature of the spin state for the Fe^{IV} sites in these complexes. Although the strong, antiferromagnetic coupling between the spins of the irons in $[(Fe^{IV}B^*)_2O]^{2-}$ precludes a direct measurement of the iron spins ($S_{1,2}$), the large, positive value for ΔE_Q unequivocally identifies them as intermediate spins, $S_1 = S_2 = 1$.

The ^{57}Fe isomer shift (δ) of $[(Fe^{IV}B^*)_2O]^{2-}$ has a small, negative value (Table 2). A comparison of this value with those for other tetra-amido Fe^{IV}−oxo complexes reveals a correlation between isomer shift and ligand charge. For example, $\delta = +0.17$ mm/s for the neutral tetramethyl tetraazacyclotetradecane (TMC) ligand in $[Fe^{IV}(TMC)O(MeCN)]^{2+}$, δ ranges from +0.04 to +0.12 mm/s for porphyrin ligands, which are dianions, in $[Fe^{IV}(porphyrin)O]^0$, and $\delta = -0.07$ mm/s for the tetra-anion B* in $[(Fe^{IV}B^*)_2O]^{2-}$.[23] Since the negative charge of these ligands is mainly located at the N atoms, it is expected that the donor capacity increases in the order TMC < porphyrin < B*. As the charge in the 4s orbital of iron increases accordingly, the isomer shift decreases, δ(TMC) > δ(porphyrin) > δ(B*).[19,24,25] Thus, the unusually small isomer shift of $[(Fe^{IV}B^*)_2O]^{2-}$ is tantamount to the exceptionally large donor strength of the TAML ligand.

3.3. Magnetic Properties. 3.3.1. Exchange Coupling and Iron−Oxo Bond Distance in $[(Fe^{IV}B^*)_2O]^{2-}$. The geometry optimization of the $[(Fe^{IV}B^*)_2O]^{2-}$ complex, which was performed for the ferromagnetic ("F") $S = 2$ system spin state, reproduced all salient features of the X-ray structure (Table 1). In particular, the calculation gives an Fe−O−Fe angle of 154.5° versus 151.4° (observed) and a torsion angle between the TAML moieties of 53.5° versus 54.0° (observed). The only structural parameter that showed a less satisfactory agreement with experimental results was the Fe−O bond length: 1.818 Å (calculated for $S = 2$) versus 1.728 Å (observed for $S \approx 0$).[26] To analyze the possibility that the discrepancy is a basis set effect, we performed a geometry optimization for the ferromagnetic state, using a basis set that includes polarization functions (see section 2). However, the extension of the basis set had only a marginal influence on the results: Fe−O = 1.803 Å, $\varphi = 54.5°$, and Fe−O−Fe = 153.4°. Next, we investigated the influence of the spin state on the Fe−O distance. We scanned the energy of the broken symmetry ("BS") state, which resembles the $S = 0$ ground state more closely than the $S = 2$ state does,

(22) Kostka, K. L.; Fox, B. G.; Hendrich, M. P.; Collins, T. J.; Rickard, C. E. F.; Wright, L. J.; Münck, E. *J. Am. Chem. Soc.* **1993**, *115*, 6746–6757.

(23) Costas, M.; Mehn, M. P.; Jensen, M. P.; Que, L., Jr. *Chem. Rev.* **2004**, *104*, 939–986.

(24) Walker, L. R.; Wertheim, G. K.; Jaccarino, V. *Phys. Rev. Lett.* **1961**, *6*, 98–101.

(25) Neese, F. *Inorg. Chim. Acta* **2002**, *337C*, 181–192.

(26) The ≈ sign is used to indicate that the distance obtained from the X-ray analysis is a Boltzmann-weighted average of the distances for $S = 0$, 1, and 2. However, since the antiferromagnetic coupling in $[(Fe^{IV}B^*)_2O]^{2-}$ is strong and the populations of the excited states with $S > 0$ are small at the temperature of the X-ray diffraction measurements (~300 K), we are effectively observing the distance for $S = 0$.

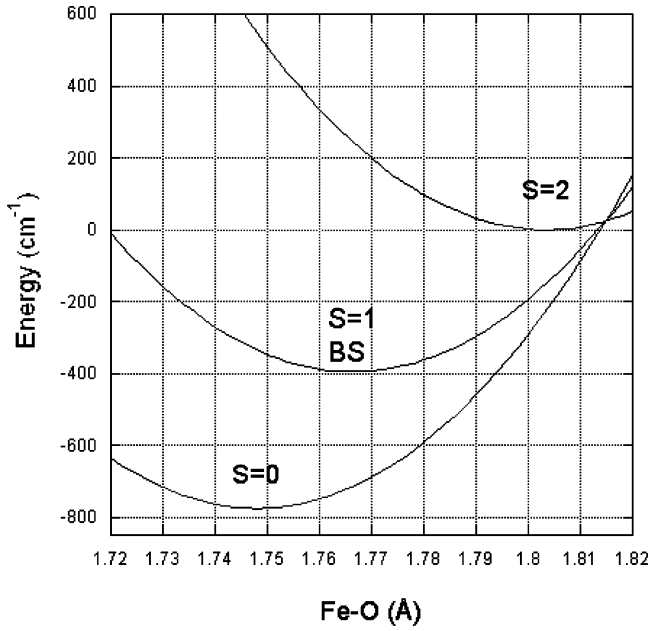

Figure 4. Energies for the system spin states of $[(Fe^{IV}B^*)_2O]^{2-}$ plotted as a function of the Fe−O distance. The curves for BS and F ($S = 2$) states were obtained by performing DFT energy scans; the curve for $S = 0$ was constructed by the procedure described in the text. The calculated Fe−O equilibrium distances are 1.803 Å ($S = 2$), 1.766 Å ($S = 1$), and 1.748 Å ($S = 0$); the X-ray value is 1.728 Å. The energies at the potential minima are given by eq 6 and are eigenvalues of the Hamiltonian in eq 7.

along the Fe−O coordinate, while keeping all other structural parameters as in the optimized structure for the ferromagnetic state. The resulting PES is shown in Figure 4 together with the potential well for the F state. Interestingly, the equilibrium Fe−O distance for the BS state, $d(\text{Fe}-\text{O})_{BS} = 1.766$ Å, is considerably shorter than the distance for the F state, yet is significantly longer than the Fe−O separation in the X-ray structure. In the present case, where one is dealing with the coupling of two spin triplets, $S_1 = S_2 = 1$, the energies of the BS state and the $S = 1$ system spin state are equal: $E_{BS} = E_{S=1}$ (see the Supporting Information). The spin dependence of the Fe−O distance calls for a geometry optimization in the $S = 0$ ground state. Unfortunately, the wave function of the antiferromagnetic $S = 0$ ground state is a linear combination of Slater determinants, which excludes a conventional DFT treatment of this state. For this reason, we have adopted a theoretical model for estimating the equilibrium Fe−O distance for the $S = 0$ ground state. We start with the conventional bilinear spin Hamiltonian for describing the exchange coupling between the paramagnetic sites in $[(Fe^{IV}B^*)_2O]^{2-}$,

$$\hat{H}_{ex} = J\hat{\mathbf{S}}_1 \cdot \hat{\mathbf{S}}_2 \tag{1}$$

The operator represents the scalar coupling of the iron spins and has an energy level scheme that obeys Landé's interval rule, $E_{S+1} - E_S = J(S + 1)$, ($S = 0, 1, 2$). In the spirit of the theory for (super) exchange interactions formulated by Anderson,[27] the exchange-coupling constant is written as

$$J = \frac{2\beta^2}{U} \tag{2}$$

where β is an effective metal-to-metal electron transfer parameter, defined in the Supporting Information, and $U > 0$ is the correlation energy, which is usually on the order of a few electron volts.[28] The model is based on the premise that β, and thus J, is a function of the Fe−O distance, $\beta = \beta[d(\text{Fe}-\text{O})]$. It is convenient to expand the squared quantity, β^2, around the equilibrium distance for the F state

$$\beta^2(x) \approx b_0 + b_1 x \tag{3}$$

where we have used the definition $x = d(\text{Fe}-\text{O}) - d(\text{Fe}-\text{O})_{F,eq}$. Obviously, $b_0 \geq 0$, and we anticipate that $b_1 < 0$ because a shortening in the Fe−O distance ($x < 0$) is expected to enhance the oxo-mediated transfer interaction between the iron sites. For systems with moderate J values, the x dependence of this parameter has little influence on the molecular geometry. However, in the present case, where the exchange coupling is unusually strong due to the short Fe−O distances, its effect on the geometry can apparently not be ignored. The dependence of J on x gives rise to different energy surfaces for the three spin states (see the Supporting Information):

$$E_{S=0}(x) \approx -\frac{6b_0}{U} - \frac{6b_1}{U}x + \kappa x^2 \tag{4a}$$

$$E_{S=1}(x) = E_{BS}(x) \approx -\frac{4b_0}{U} - \frac{4b_1}{U}x + \kappa x^2 \tag{4b}$$

$$E_{S=2}(x) = E_F(x) = \kappa x^2 \tag{4c}$$

where the minimum of the potential energy surface for the F state has been taken as the origin of the energy scale. κ is the elastic force constant for the Fe−O stretch. The antiferromagnetic exchange vanishes in the F state because the metal-to-metal transfer interactions leading to this interaction are Pauli-forbidden in this state.[29] We identify the expressions in eqs 4b (BS) and 4c (F) with the potential energy surfaces obtained by the DFT scans for these states (Figure 4). This allows us to estimate the values of the coefficients κ, b_0/U, and b_1/U, which can subsequently be used to evaluate the potential surface for the ground state, $E_{S=0}(x)$ (eq 4a). The force constants deduced from the DFT calculations for the F and BS states are practically equal ($\kappa_{BS} = 1.75 \times 10^5$ cm^{-1}/Å^2, $\kappa_F = 1.79 \times 10^5$ cm^{-1}/Å^2, see the Supporting Information), which justifies the use of the same value for the effective force constants in eqs 4a−c.

The minima of the energy surfaces in eqs 4a−c are located at

$$x_{S=0} \approx \frac{3b_1}{\kappa U} \tag{5a}$$

$$x_{S=1} = x_{BS} \approx \frac{2b_1}{\kappa U} \tag{5b}$$

$$x_{S=2} = 0 \tag{5c}$$

Using the DFT equilibrium distances for the F and BS states, we obtain $x_{BS} = -0.037$ Å, which together with $\kappa =$

(27) Anderson, P. W. *Solid State Phys.* **1963**, *14*, 99–214.

1.79×10^5 cm^{-1}/Å^2 yields $b_1/U = -3312$ cm^{-1}/Å. The DFT calculations at the equilibrium geometry for the F state yield 152 cm^{-1} for the exchange splitting separating the F and BS state energies. The splitting can be identified with the difference $E_F(0) - E_{BS}(0) = 4b_0/U$, from which it follows that $b_0/U = 38$ cm^{-1}. Substitution of these parameter values into eq 5a gives $x_{S=0} = -0.055$ Å. By combining this value with the DFT equilibrium distance for the F state, $d(\text{Fe}-\text{O})_{F,eq} = 1.803$ Å, we obtain the equilibrium distance $d(\text{Fe}-\text{O})_{S=0,eq} = 1.748$ Å for the $S = 0$ ground state. The predicted Fe−O distance is in good agreement with the value 1.728 Å deduced from the crystal structure; an overlay of the geometry predicted for $S = 0$ and the X-ray structure of $[(Fe^{IV}B^*)_2O]^{2-}$ is presented in Figure 1D. In this model, the contraction of the Fe−O distance is driven by the distance dependence of the antiferromagnetic stabilization energy, which increases as a function of decreasing spin.

3.3.2. Spin Densities. The atomic spin densities for $[(FeB^*)_2O]^{2-}$, given in section 2.2, show the following properties: (i) the spin densities at B* and its coordinating iron have opposite signs; (ii) the spin populations for the irons in the F state are greater than the number of unpaired electrons, SP > 2; (iii) the spin density at B* is mainly accommodated by the amido atoms and benzene moiety; (iv) the spin density at B* in the F state is larger in magnitude than in the BS state throughout the Fe−O range 1.7−1.8 Å. Properties i and ii are unlike what is normally found for covalent metal-to-ligand spin delocalization.[30] Property iii suggests that the FeB* moieties in $[(FeB^*)_2O]^{2-}$ possess some iron(III)-radical character, due to admixture of the $|\{Fe^{III}(S'_i = {}^3/_2), \dot{B}^*(S''_i = {}^1/_2)\}S_i = 1>$ configurations (i = 1, 2) into the electronic state. Interestingly, properties i−iii are retained when the benzene moiety is replaced by an alkene (Figure 2), indicating that the negative spin polarization of the ligand is not resulting from the noninnocence bestowed on B* by the benzene moiety. Similarly, as for the B* complex, the alkene-substituted species has a long Fe−O distance of ∼1.80 Å in the F state. Property iv suggests that the admixture of the radical state in the F state is larger than in the BS state. Given that the radius of iron(III) is larger than for iron(IV), an increase in the admixture of the radical configuration in the F state could result in a larger Fe−O bond length for this state. In such a scenario, the structural relaxation, which was ascribed to a dependence of resonance parameter β on the Fe−O distance in section 3.3.1, may arise from the spin (S) dependence of the amount of iron(III)−B*(radical) character admixed in the wave function. One could speculate that in the F state, where there is no cancellation of spin density at the bridging oxygen (or at the metals by the exchange of opposite spin density) as in the BS state (see section 2.2), the exchange fields in the Fe−O fragments are stronger than in the BS state, attracting additional positive spin density from TAML to iron and increasing the negative spin density on the ligands. With the caveat that a quantitative expression for the energetics of this spin polarization mechanism is presently lacking, we note that the formalism of section 3.3.1 is general in the sense that it can be applied to any spin-dependent relaxation mechanism that can be represented by adding a linear term in Fe−O distance to exchange parameter J.

3.3.3. Biquadratic Exchange. The energies at the minima of eqs 5a−c are given by the expression

$$E_S(x_S) \approx c + \left(\frac{b_0}{U} + \frac{3b_1^2}{\kappa U^2}\right)S(S+1) - \frac{b_1^2}{4\kappa U^2}[S(S+1)]^2 \quad (6)$$

where $S = 0$, 1, and 2 and c is a spin-independent constant. In addition to a term linear in $S(S+1)$, eq 6 contains a quadratic term, leading to deviations from Landé's interval scheme. The energies in eq 6 can be interpreted as the eigenvalues of a biquadratic spin Hamiltonian[31−33]

$$\hat{H}_{ex} = c' + j_0\hat{\mathbf{S}}_1\cdot\hat{\mathbf{S}}_2 + j_1(\hat{\mathbf{S}}_1\cdot\hat{\mathbf{S}}_2)^2 \quad (7)$$

of which the coupling constants are defined as

$$j_0 = \frac{2b_0}{U} + \frac{2b_1^2}{\kappa U^2} \quad (8a)$$

$$j_1 = -\frac{b_1^2}{\kappa U^2} \quad (8b)$$

Substitution of the values for κ, b_0/U, and b_1/U, obtained from the DFT results for the F and BS states, into eqs 8a and 8b gives the values $j_0 = 199$ cm^{-1} and $j_1 = -61$ cm^{-1}. The origin of the large biquadratic term in $[(Fe^{IV}B^*)_2O]^{2-}$ can be understood as follows. Equation 1, with $J = J(x)$, implies that the spin-state energies in eqs 4a−c obey the Landé rule at any value for x. For example, at $x = 0$ (i.e., the equilibrium distance for $S = 2$), the energies are described by a bilinear Hamiltonian (eq 1) with $J = 2b_0/U = 76$ cm^{-1}, such that $E_{S=1}(0) - E_{S=0}(0) = 76$ cm^{-1}. However, the spin-state energies evaluated at their respective minima (eq 6) give a much larger difference: $E_{S=1}(x_{S=1}) - E_{S=0}(x_{S=0}) = 381$ cm^{-1}. The energy associated with the spin-dependent structural relaxation in $[(Fe^{IV}B^*)_2O]^{2-}$ is the main contribution to the splitting between the $S = 1$ excited state and the $S = 0$ ground state: 381 − 76 cm^{-1} = 305 cm^{-1}. By including the reorganization energy, we obtain for the splitting between the $S = 2$ and $S = 0$ states the energy $E_{S=2}(0) - E_{S=0}(x_{S=0}) = 775$ cm^{-1}. We observe that the ratio $[E_{S=2}(0) - E_{S=0}(x_{S=0})]/[E_{S=1}(x_{S=1}) - E_{S=0}(x_{S=0})] \approx 2$, obtained with the biquadratic Hamiltonian (eq 7), is considerably smaller than the Landé ratio of 3 predicted on the basis of the bilinear Hamiltonian (eq 1).

Conclusions

The conclusions of this work can be summarized as follows: (i) Torsion φ in $[(Fe^{IV}B^*)_2O]^{2-}$ (Figure 1B) is caused by hydrogen bonding between the FeB* moieties.

(28) We assume that the ferromagnetic term in $J = J_F + J_{AF}$ is small compared to the antiferromagnetic term, such that $J \approx J_{AF}$.

(29) We refer here to the transfer interactions involving the half-filled xz and yz orbitals of the Fe^{IV} ions.

(30) Popescu, D.-L.; Chanda, A.; Stadler, M.; Tiago de Oliveira, F.; Ryabov, A. D. Münck, E.; Bominaar, E. L.; Collins, T. J. *Coord. Chem. Rev.* **2007**. In press.

(31) Kittel, C. *Phys. Rev.* **1960**, *120*, 335–342.

(ii) The bent conformation of Fe−O−Fe in $[(Fe^{IV}B^*)_2O]^{2-}$ is an intrinsic property of this unit. (iii) The Fe−O distance depends on the system spin, *S*. The dependence has two corollaries: (a) the exchange splitting between the energies of the spin states is in part due to structural reorganization, and (b) the conventional bilinear spin Hamiltonian has to be extended with a biquadratic term (eq 7) to accommodate the structural reorganization energies.

(32) Bean, C. P.; Rodbell, D. S. *Phys. Rev.* **1962**, *126*, 104–115.
(33) Harris, E. A.; Owen, J. *Phys. Rev. Lett.* **1963**, *11*, 9–10.

Acknowledgment. This work was supported by N.S.F Grant MCB 0424494 (to E.M.), the Heinz Endowments (T.J.C.), and the U.S. EPA (Grant RD 83 to T.J.C.).

Supporting Information Available: Figures S1 and S2 (section S.1) and details concerning the relation between Fe−O distance and spin state (section S.2), broken symmetry state (section S.3), and Hückel model for Fe−O−Fe bond angle (section S.4). This material is available free of charge via the Internet at http://pubs.acs.org.

IC800881P